(Received 6 November 2024, Accepted 16 December 2024, Scheduled 17 December 2024)

Separation of a Toroidal Mode in Clusters of Dielectric Particles

Tong Wu[1], Andrey B. Evlyukhin[2], and Vladimir R. Tuz[1, 3, *]

[1]*State Key Laboratory on Integrated Optoelectronics, College of Electronic Science and Engineering International Center of Future Science, Jilin University, 2699 Qianjin Street, Changchun 130012, China*
[2]*Institute of Quantum Optics, Leibniz University Hannover, Welfengarten 1, Hannover 30167 Germany and Cluster of Excellence PhoenixD, Leibniz University Hannover, Welfengarten 1A, Hannover 30167, Germany*
[3]*School of Radiophysics, Biomedical Electronics and Computer Systems, V. N. Karazin Kharkiv National University 4, Svobody Square, Kharkiv 61022, Ukraine*

ABSTRACT: Constructing and utilizing toroidal modes in clusters of dielectric particles opens pathways to creating more efficient, compact, and functional devices across various fields, from sensing and telecommunications to energy and defense applications. Toroidal modes contribute to unusual material properties related to artificial magnetism, which is essential for designing innovative metamaterials. In this paper, we establish a relationship between eigenoscillations (modes) and scattering characteristics of a toroidal dielectric particle (torus) and clusters of particles composed of different numbers of dielectric disks arranged in a circular configuration (rings) in terms of the manifestation of their toroidal response. In particular, we examine the multipole contributions to the scattering cross-sections obtained in the exact form and long-wavelength approximation. A toroidal mode is introduced as a mode of the system for which the second-order term related to the exact electric dipole in the multipole decomposition is much greater than the first-order term. We show that the individual modes of the torus and hybrid modes of the ring consisting of an electromagnetically coupled ensemble of particles can be uniquely related, including the lowest-frequency toroidal dipole mode. Unlike the torus, the toroidal dipole mode in the ring can be separated in frequency from other multipole contributions, allowing excitation of the pure toroidal dipole resonance when providing corresponding irradiation conditions for external electromagnetic waves. This study provides an opportunity to better understand the physics of toroidal resonances in structures containing ensembles of dielectric particles and the peculiarities of their application in advanced microwave and photonic systems.

1. INTRODUCTION

In recent years, a novel approach based on utilizing Mie resonances in dielectric nanostructures (metamaterials) has gained great attention for efficient control of the amplitude, phase, and polarization of propagated light [1]. Due to the wide variety of their optical features and ability to enhance the light-matter interaction, the implementation of such nanostructures has led to a new paradigm in photonics, called "Mie-tronics" — Mie resonant metaphotonics [2, 3]. In particular, many effects supported by dielectric nanostructures, such as bound states in the continuum, optical anapole, superscattering, and perfect absorption, have led to the emergence of such innovative devices as metalenses, nanoantennas, nanolasers, and advanced chemical and biological sensors, to name a few (see comprehensive review papers [4–6] and references therein).

Dielectric metamaterials are typically made of high-refractive index dielectric particles supporting Mie-type resonances of electric and magnetic nature [7–9]. They are geometry- and size-dependent resonances occurring in particles [10] when the wavelength of light inside the dielectric body (resonator) becomes comparable to its spatial dimensions (e.g., radius). From the electromagnetic theory viewpoint, the interaction of light with such structures is described within the framework of the multipole decomposition method [11], where resonances are related to a set of spherical (i.e., dipolar, quadrupolar, octupolar, etc.) harmonics supported by the resonator. This method is also applicable to relatively complex and composite particles, as well as their aggregates and clusters [12].

Although Mie-tronics is related to the development of high-performance nano-optical components, the theory of dielectric resonators was first introduced in microwave technologies related to dielectric resonator antennas [13, 14]. Engineering of such antennas requires information on basic quantities such as the radiated fields, resonant frequency, bandwidth, quality factor, and field distribution inside the resonator. The design is based primarily on the analysis of eigenoscillations (modes) of the resonator and the choice of the corresponding method for their excitation. These eigenoscillations are typically classified as the transverse electric (TE), transverse magnetic (TM), and hybrid (HE, EH) modes [15]. An important feature of isolated dielectric antennas is that, in general, the different modes of a resonator radiate like electric and magnetic multipoles. For example, it is well known that the $TE_{01\ell}$ mode of an isolated cylindrical resonator radiates like a magnetic dipole oriented along its axis. Similarly, the $HE_{11\ell}$ and $EH_{11\ell}$ modes radiate

* Corresponding author: Vladimir R. Tuz (tvr@rian.kharkov.ua).

like a horizontal magnetic and electric dipole, respectively (see Table 1 in [15]; in the mode abbreviations, the first, second, and third indices denote the order of the azimuthal, radial, and vertical variations of the fields; here we do not fix the exact number for ℓ).

In systems containing ensembles of particles, due to electromagnetic coupling between them, the modes of individual particles hybridize into cluster modes [16]. The higher-order contributions may be dominant in the scattered field of such composite particles. In particular, for clusters with toroidal topology (e.g., rings), such a dominant contribution can be a toroidal dipole moment [17–24], which is a second-order term of the exact electric dipole moment [25, 26] (toroidal modes are characterized by circulating magnetic fields that form a closed-loop torus). Structures supporting a toroidal response are of particular interest in photonics because such modes can provide enhanced light manipulation [27], reduced scattering [28], high sensitivity in bio- and chemical sensors [29, 30], and nonlinear operations in photonic devices [31]. Nevertheless, manipulating toroidal modes in clusters of dielectric particles presents several challenges due to the intricate nature of these modes and their dependence on precise configurations. Toroidal modes are generally weak and challenging to excite compared to electric or magnetic dipoles, requiring sophisticated incident wave patterns or coupling mechanisms. Moreover, competing electromagnetic modes, such as electric or magnetic dipoles, can interfere with the toroidal mode, reducing its prominence [33].

It should be noted that the mode composition and scattering by toroidal objects have been the subject of fairly close study for a long time in various fields, from plasma physics, microwave and optical waveguides [34–44] to atmospheric and space phenomena [45, 46]. In particular, modes of a torus with perfectly conducting walls were classified in Ref. [47], and their three types were identified. These modes were derived involving the toroidal coordinates [48]. Regarding microwave devices, using toroidal modes offers exciting possibilities for advancing technologies in telecommunications, sensing, and stealth systems. Their high-quality factors make them ideal for microwave resonators used in oscillators, filters, and frequency-selective surfaces [32]. Interest in toroidal objects has also emerged in plasmonics, where the modes of metallic torus have been studied in Refs. [49–52].

The most relevant attempt to clarify the manifestation of a toroidal dipole resonance in a toroidal dielectric particle was undertaken in [53]. The results indicate that a moderate major radius should be set for a dielectric torus to observe the isolated toroidal dipole resonance. It is also noted that the toroidal resonance can be maintained in a dielectric torus for a wide choice of materials. Still, the best results are obtained for a torus with a higher contrast between the dielectric material and the surrounding medium. Otherwise, a significant contribution from the electric dipole is present in the scattered field. High permittivity materials are easily accessible in the microwave range but not so widespread in optics; however, the authors confirmed their results also for a torus made of $LiTaO_3$ operated in the range of 1.35–1.55 THz. However, when shifted to the higher frequencies, fabrication constraints, material losses, and nonlocality should be accounted for [54].

Seminal papers on toroidal metamaterials consider structures whose unit cells contain clusters of particles arranged in a ring to provide the necessary head-to-tail distribution of magnetic dipole moments associated with these particles [55, 56]. In our recent works [57, 58], we supposed that the toroidal response of such clusters may be related to modes of a solid torus derived in Ref. [47]. The goal of the present paper is a sequential detail study of modes and scattering characteristics of a solid torus and a commensurate inhomogeneous ring consisting of an ensemble of particles to reveal these systems' similar and distinctive features in the manifestation of toroidicity. We show that unlike solid tori, ring structures of particles have additional degrees of freedom for tuning and controlling the resonant toroidal response, which makes them very attractive for metaphotonics. The study uses the secondary multipole decomposition (SMD) method developed earlier [59, 60] to reveal multipole contributions of separate elements in the field scattered by complete clusters. To maintain continuity with previous studies [21–23, 53, 57], here we consider structures made of ceramic particles operated in the microwave range (7–16 GHz).

2. PROBLEM DESCRIPTION

In what follows, we compare the modal composition and scattering characteristics of two structures: a solid torus and a commensurate ring composed of several resonators. The major and minor radii of the torus are R and R_d, respectively. We keep the ring's radius corresponding to the torus's radius. Also, constitutive disks forming the ring have a radius R_d and a height H_d (see Fig. 1). All geometrical parameters of the structures under study are set on the millimeter scale, so the corresponding resonances appear in the microwave range. The number of the disks in the ring is N. To create a symmetric structure resembling a toroid, the disks are distributed in the ring at approximately the same distance from the boundaries of the toroid planes so that any pair of opposite faces of the disks are parallel to these boundaries.

We assume that the structures under study are made from a non-magnetic material with a relative permittivity ε. They are located in an air-like environment with constitutive parameters $\varepsilon_s = 1$. To identify comparable features of the structures, their identical electromagnetic conditions should be ensured. Thus, we relate the permittivity of the inhomogeneous ring composed of disks ($\varepsilon = \varepsilon_{\text{disk}}$) separated by gaps ($\varepsilon_{\text{gap}} = \varepsilon_s$) to the permittivity of the torus ($\varepsilon = \varepsilon_{\text{torus}}$) at fixed R and R_d. In this case, $\varepsilon_{\text{disk}}$ must be additionally determined depending on the height H_d of the disks and their number N in the ring. This can be done involving the Maxwell-Garnet mixing rule [61], which gives the effective permittivity of the composite structure in terms of the relative permittivities and volume fractions of its individual constituents (see also relevant paper [62], where the toroidal samples made of cubic inclusions have been described with the effective medium theory and experimentally studied at microwaves).

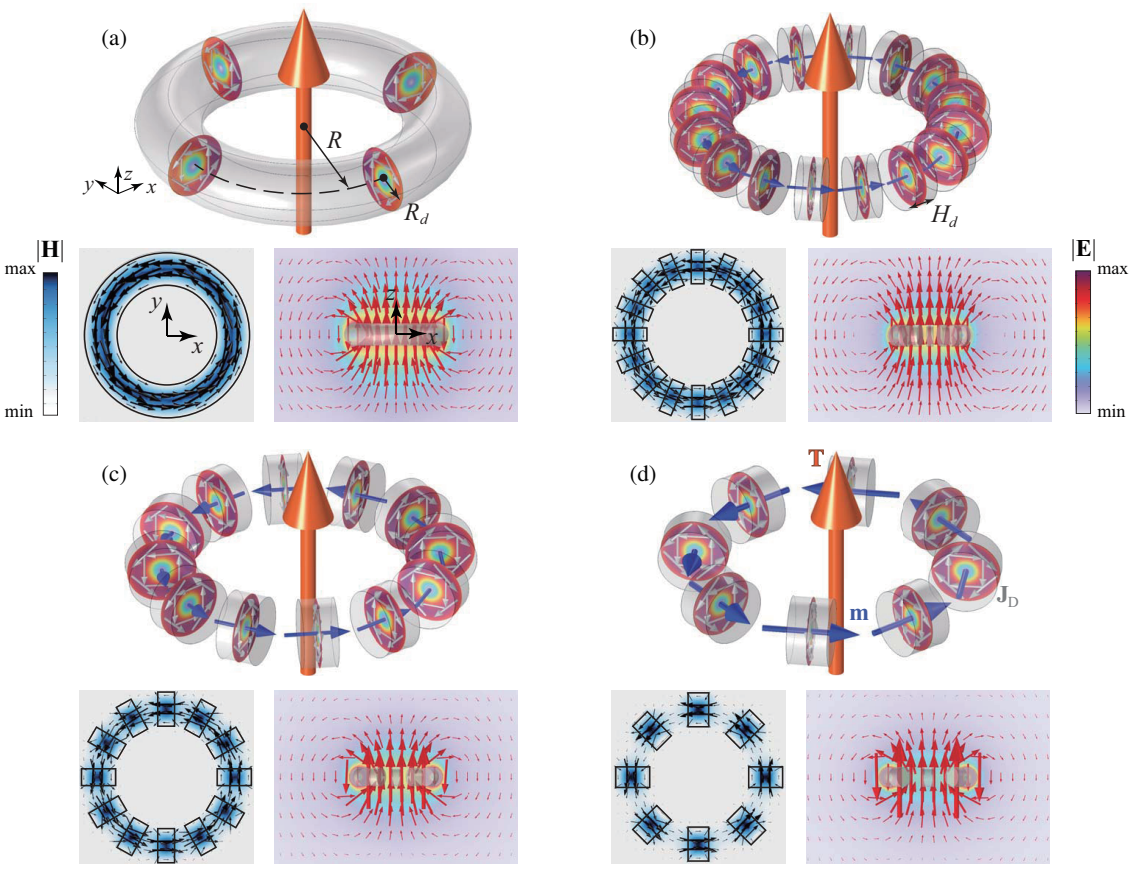

FIGURE 1. Artistic view of the geometry of (a) a solid dielectric torus and rings composed of (b) $N = 16$, (c) $N = 12$, and (d) $N = 8$ dielectric particles (disks) and eigenfield patterns of the toroidal mode. The origin of the Cartesian coordinate system coincides with the torus (ring) center. Grey, blue, and orange arrows show the displacement current $\mathbf{J}_D$ flow and orientation of the magnetic **m** and toroidal **T** dipole moments, respectively. Cold (hot) color maps and black (red) arrows are related to the magnitude and flow of the magnetic (electric) eigenfield. The toroidal nature of the mode is determined by the circular flow of the magnetic field strongly localized inside the torus and the flow of the electric field indistinguishable from the distribution produced by the conventional electric dipole. The major and minor radii of the torus are $R = 4.0\,\text{mm}$ and $R_d = 1.0\,\text{mm}$, respectively, while $\varepsilon_{\text{eff}} = \varepsilon_{\text{torus}} = 60$. Parameters of the disks are (b) $H_d = 0.8\,\text{mm}$ ($\varepsilon_{\text{disk}} \approx 116.85$), (c) $H_d = 1.0\,\text{mm}$ ($\varepsilon_{\text{disk}} \approx 124.57$), and (d) $H_d = 1.2\,\text{mm}$ ($\varepsilon_{\text{disk}} \approx 155.46$).

Following the Maxwell-Garnet mixing rule, the effective permittivity ε_{eff} of the ring can be written as:

$$\varepsilon_{\text{eff}} = \frac{NV_{\text{disk}}\varepsilon_{\text{disk}} + (V_{\text{torus}} - NV_{\text{disk}})\varepsilon_{\text{gap}}}{V_{\text{torus}}}, \tag{1}$$

where $V_{\text{torus}} = 2\pi^2 RR_d^2$ [63] and $V_{\text{disk}} = \pi R_d^2 H_d$ are volumes of the torus and disk, respectively, and $\varepsilon_{\text{gap}} = \varepsilon_s$.

Substitution of expressions for volumes in Eq. (1) and simple algebraic operations yield

$$\varepsilon_{\text{eff}} = \varepsilon_s + NH_d\frac{\varepsilon_{\text{disk}} - \varepsilon_s}{2\pi R}. \tag{2}$$

Then, the required relative permittivity of the disks $\varepsilon_{\text{disk}}$ is equal to

$$\varepsilon_{\text{disk}} = \frac{2\pi R}{NH_d}\varepsilon_{\text{torus}} - \frac{2\pi R - NH_d}{NH_d}\varepsilon_s, \tag{3}$$

where we set $\varepsilon_{\text{eff}} = \varepsilon_{\text{torus}}$.

After determining the permittivity $\varepsilon_{\text{disk}}$, one can solve the problems on the modes and scattering characteristics of a homogeneous torus and an inhomogeneous ring, where the number of disks N and their height H_d can be subjected as parameters. In our study, all subsequent simulations related to these two problems are carried out in the COMSOL Multiphysics software [64]. The spherical computational domain of our model includes the structure placed in a surrounding space truncated by a perfectly matched layer (PML). The PML is added to the model to simulate open (infinite) space and prevent unwanted re-reflections of waves within the computation domain. The origin of the Cartesian coordinate system coincides with the center of the structure. In this study, we use the default physics-controlled COMSOL settings for fine mesh generation.

These solutions have been supplemented by the equations of the multipole decomposition method (see Refs. [22, 65, 66] and Appendix A) which are implemented in COMSOL as corresponding calculation procedures. We utilize these equations given in both exact form and long-wavelength approximation (LWA).

3. EIGENOSCILLATIONS CONDITIONS

In the first stage of our study, we conduct a numerical analysis of the spectrum of the eigenfrequencies of a solid torus and an inhomogeneous ring. Eigenfrequencies (or natural frequencies) are specific discrete states where a system tends to resonate when the incident field frequency coincides with the system's eigenfrequency. A dielectric resonator has a spectrum of eigenfrequencies related to the corresponding modes (types of oscillations). These modes are determined by the resonator's geometry and material properties. The eigenfrequencies can be determined by solving the Helmholtz equation with the appropriate boundary conditions (the behavior of fields at the boundaries of the dielectric material, such as the continuity of the electric and magnetic fields determines the allowable modes). In particular, the solver finds a solution to the eigenproblem as a complex angular frequency given in the form $\omega = \omega' + i\omega''$, where a real part ω' represents the eigenfrequency, and an imaginary part ω'' is responsible for the damping (since the dielectric resonator is an open electromagnetic system, there is always energy leakage through the walls of the resonator even in the absence of material losses). After finding the eigenfrequency, the solver allows one to plot the patterns of the mode eigenfield. Thus, based on the eigenfield characteristic, the modes of the structures under study can be classified, and the corresponding mode bearing the toroidal dipole response can be revealed by analyzing the multipole content. The multipole decomposition is performed by integrating the mode eigenfield over the structure volume.

Therefore, to find out the mode of interest, we analyze both the eigenfield distributions and the magnitudes of the multipole terms. First of all, among the modes released by the solver, those are picked out that demonstrate a circular (vortex-like) flow of the magnetic field inside the structure. This distribution of the magnetic field is ensured by the poloidal flow of polarization (displacement) currents in the cross-section of the torus, which is a necessary sign of toroidicity. Then, a particular mode is selected based on the multipole contribution analysis. The knowledge of the multipole composition of the mode allows us to determine the external irradiation conditions required for the excitation of this mode [67].

In the framework of the multipole decomposition method derived in terms of spherical harmonics, an exact electric dipole moment ($\mathrm{ED}^{\mathrm{total}}_{\mathrm{exact}}$) is expressed with the direct inclusion of the toroidal counterpart [25]. Among the selected modes having a suitable eigenfield distribution, we define the toroidal dipole mode as a state where the second-order term [toroidal dipole (TD) moment, $\mathbf{T}$] in the expansion of the exact electric dipole moment dominates over the first-order one [quasistatic electric dipole (ED) moment, $\mathbf{p}_0$], $|\mathbf{p}_0| \ll \eta|\mathbf{T}|$, with negligible contributions from the remaining components in the decomposition derived in the LWA (see, Eq. (A2) in Appendix A and Refs. [57, 58]).

A specific eigenfield of the selected toroidal dipole mode existing in a dielectric torus is shown in Fig. 1(a). One can also relate this mode to the mode of the first type with index $m = 0$ for a toroidal cavity with a perfectly conducting wall derived by solving the Helmholtz equation in the toroidal coordinate frame (see Fig. 5 in Ref. [47]). The distribution of the electric far field for the given mode does not differ from the field of an electric dipole, which is also a key signature of the toroidal resonance [25].

Since we consider commensurate structures, this guarantees the spectral proximity of the corresponding eigenfrequencies for the torus and ring modes. The eigenfield patterns for the corresponding modes in the ring should also be similar to those in the torus. By these features, the toroidal dipole mode of several rings different in the parameters N and H_d are found and plotted in Figs. 1(b)–(d) (although this does not affect the overall characteristics of the structure, here we consider rings containing an even number of particles ($N = 8$, 12, 16) so that the field patterns appear symmetrical in the figures just for convenience).

The ring of dielectric disks creates a closed-loop structure, facilitating the excitation of a toroidal dipole moment. Unlike the mode of the solid torus, the mode of the given inhomogeneous ring is the result of interactions between specific modes of the constitutive disks existing due to electromagnetic coupling between the particles [57]. In particular, the obtained eigenfield patterns suggest that the lowest-order transverse electric (TE) mode is maintained in each disk which is characterized by a circular flow of the displacement current around the central axis of the disk ($\mathrm{TE}_{01\ell}$ mode; see the mode nomenclature of the disk-shaped resonators in [15]).

The SMD allows revealing the contribution of the multipoles of the constituent parts of the composite structure to its overall multipole moments (see Appendix B). From the distribution of the electric field in the disks shown in Fig. 1, it follows that the main multipole moment on each disk with a number n is the individual magnetic dipole (MD) moment $\mathbf{m}_n$ directed along the disk axial axis. For the ring structures, an ensemble of the MD moments acquires a head-to-tail arrangement in the whole ring. From the SMD [see Eq. (B1)] such an arrangement produces a collective (hybrid) mode of the ring manifesting in a toroidal dipole moment $\mathbf{T}$ of the overall structure, where

$$\mathbf{T} \simeq \sum_{n=1}^{N} [\mathbf{r}_n \times \mathbf{m}_n], \tag{4}$$

is its main multipole moment.

The correspondence between the torus and ring modes is confirmed by the distribution of both the magnetic and electric eigenfields. The electric field associated with the toroidal dipole mode forms closed loops around the circular axis of the ring, creating a pattern where the magnetic field circulates. This results in a net zero MD moment while maintaining a non-zero TD moment. Nevertheless, the mode of the ring exhibits resonant behavior at specific frequencies, determined by the size, spacing, and dielectric properties of the disks. It may result in complex behavior and potential frequency shifts. To reveal this peculiarity, the eigenfrequency, quality factor, and ED and TD contributions of the toroidal dipole mode for the given structures are calculated as functions of the permittivity $\varepsilon_{\mathrm{torus}}$. The results are collected in Fig. 2 (to estimate the magnitudes of other contributions such as the magnetic dipole (MD), elec-

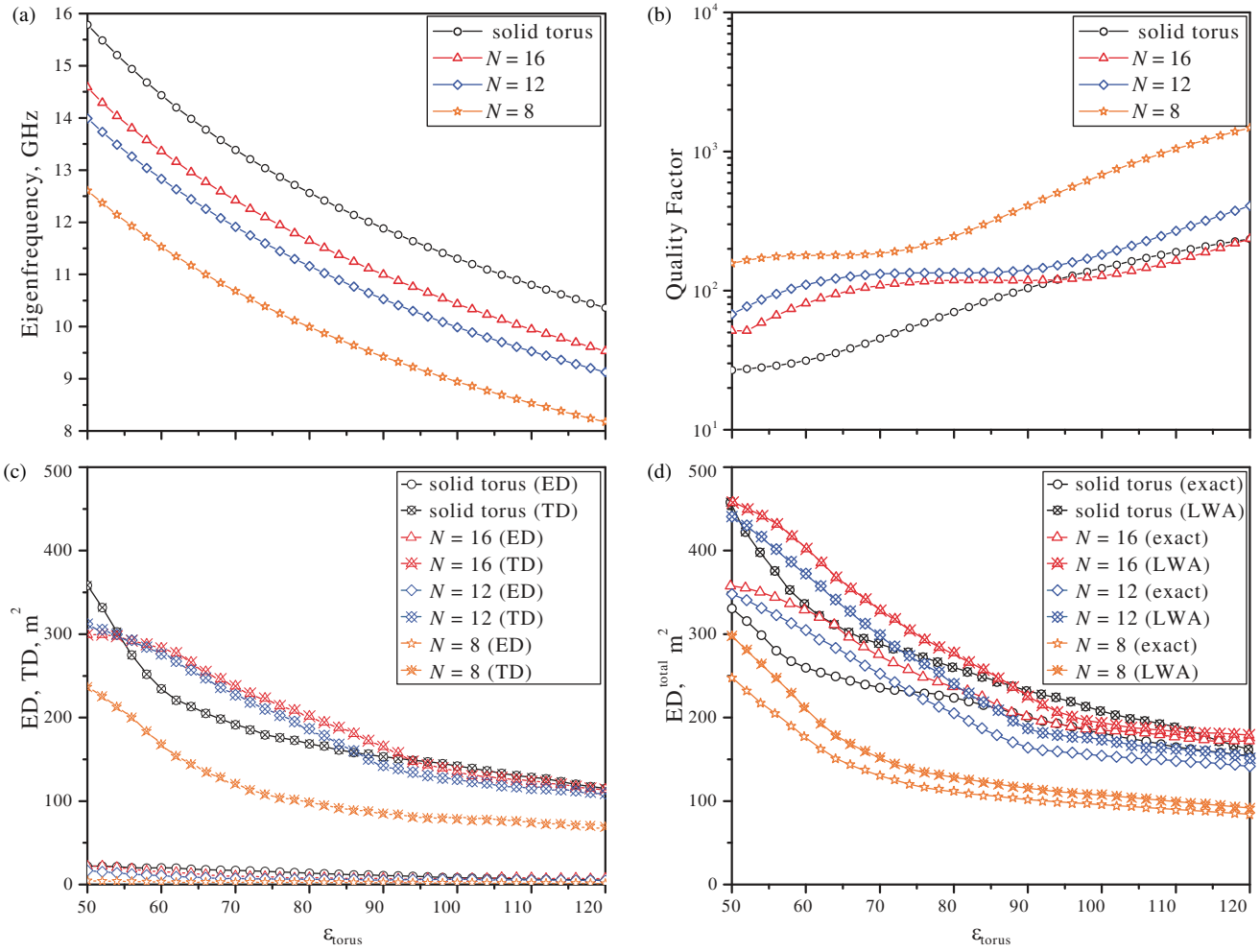

FIGURE 2. Dependence of the (a) eigenfrequency, (b) quality factor, (c) ED and TD contributions calculated in the LWA, and (d) ED^{total} calculated in the LWA and exact form on the relative permittivity ($\varepsilon_{eff} = \varepsilon_{torus}$) for the structures presented in Fig. 1. The quality factor of the mode is derived from the eigenfrequency ω' and damping ω'' as $Q = \omega'/2\omega''$.

tric quadrupole (EQ), and magnetic quadrupole (MQ) in the toroidal mode of the ring, see also Fig. 1 in Ref. [57]).

From Fig. 2(a) it follows that, although the eigenfrequencies in the solid torus and the commensurate inhomogeneous ring are closely spaced, they are a bit different, where the eigenfrequency of the torus is higher than that of the ring. The difference in the eigenfrequencies increases with decreasing the number of disks forming the ring. However, this difference remains constant with increasing ε_{torus} (we recall that we fix here $\varepsilon_{eff} = \varepsilon_{torus}$, therefore $\varepsilon_{torus} < \varepsilon_{disk}$). As the permittivity increases, the eigenfrequencies decrease, in full accordance with classical electromagnetism predictions.

The dependence of the mode quality factor on permittivity has a more complex behavior, as Fig. 2(b) suggests. The quality factor of the mode of the inhomogeneous ring is higher than that of the homogeneous torus, which is apparently determined by the higher permittivity of the constitutive disks providing a better electromagnetic field confinement in dielectric resonators. This also explains the higher quality factor of structures with fewer disks. It is noteworthy that for the ring there are ranges when the quality factor has a flat characteristic without any gradient with increasing permittivity, whereas for the torus there is always a monotonic increase in the quality factor of the mode.

To explicitly confirm the toroidal nature of the given mode, we verified that the TD contribution dominance in its eigenfield persists with increasing permittivity. In Fig. 2(c) it can be seen that the magnitudes of both ED and TD contributions decrease as ε_{torus} increases where ED tends to zero, while the overall electromagnetic response of all structures approaches quasi-static conditions. The approach to quasi-static conditions is also confirmed by Fig. 2(d), which shows a comparison of the magnitude of the total electric dipole moment $ED^{total} = ED + TD$ obtained in the exact form and LWA. As expected, these two solutions converge with increasing permittivity for the modes of both the torus and ring.

4. SCATTERING CHARACTERISTICS

At this stage of our study, we proceed to identify the scattering characteristics of the given structures in the frequency range of the existence of the toroidal dipole mode. The ex-

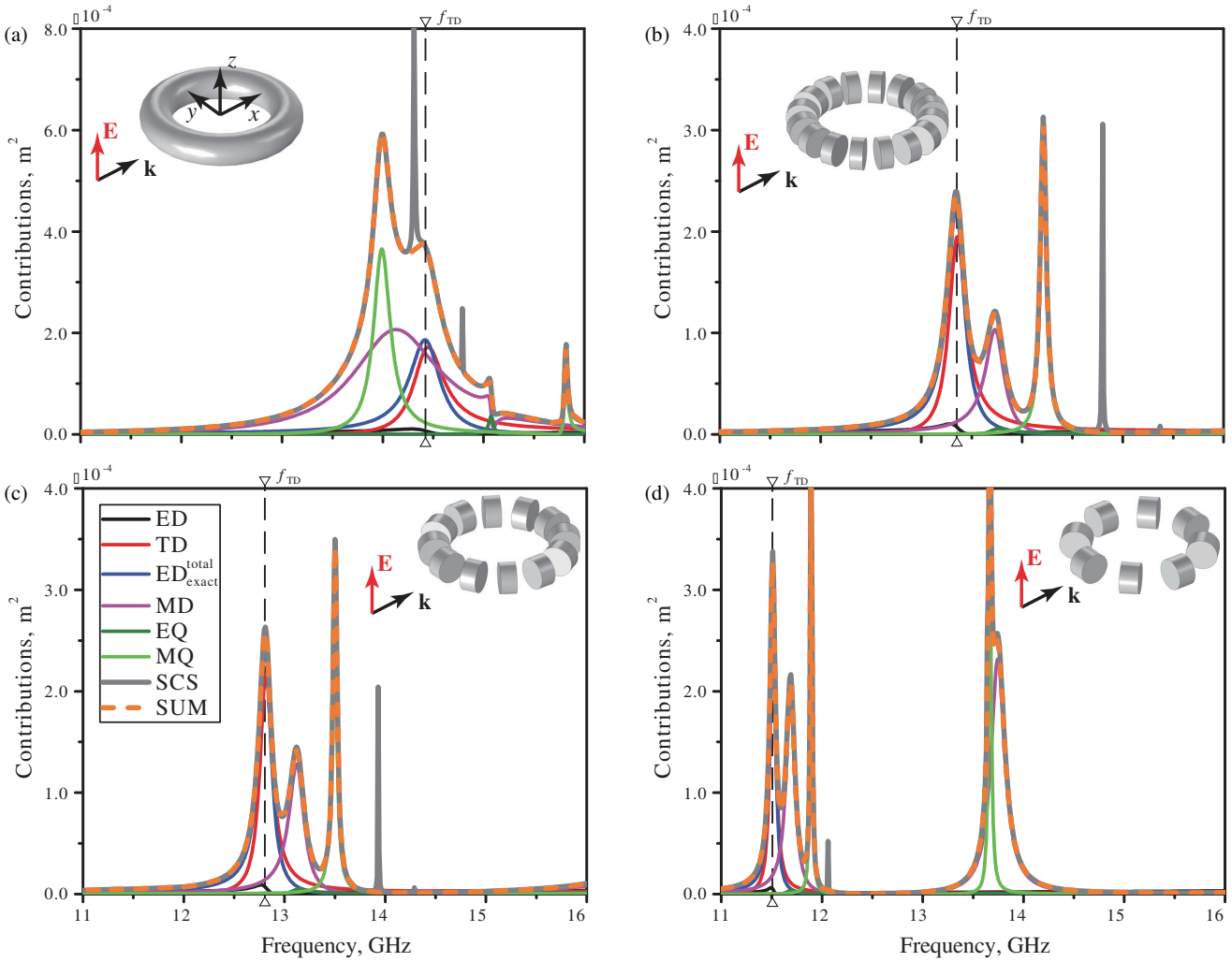

FIGURE 3. Scattering cross-section (SCS) and corresponding multipole decomposition contributions calculated for (a) solid dielectric torus and rings composed of (b) $N = 16$, (c) $N = 12$, and (d) $N = 8$ dielectric particles (disks). The incidence condition and polarization of the irradiating wave are given in the insets. The caption of Fig. 1 lists all geometrical and material parameters of the structure.

citation of the toroidal dipole mode in the structure occurs via its resonant interactions with irradiating waves under their specific incidence conditions and polarization. In particular, since the dynamic toroidal dipole moment is a part of the exact electric dipole moment, the linearly polarized wave can excite the toroidal dipole mode in the structure when the direction of its electric field vector **E** coincides with the vector **T** belonging to the mode [56, 57]. Further, in the given coordinate frame, we assume that lateral irradiation of the structures by a z-polarized plane electromagnetic wave propagated along the x-axis ($\mathbf{E} = \{0, 0, E_z\}$, $\mathbf{k} = \{k_x, 0, 0\}$, $k = 2\pi f/c$, where $f \in [9, 16]$ GHz is the frequency of the incident wave, and c is the speed of light in vacuum).

The calculation of the scattering cross-section in the solver is performed in two alternative ways: (i) deriving the scattered energy by integrating the Poynting vector over an imaginary sphere constructed around the particle in the far-field zone (SCS), and (ii) deriving the scattering cross-section by summing the dipole and quadrupole contributions (SUM), Eq. (A2). In the latter case, the multipole contributions are calculated in the LWA, while the total electric dipole moment ($\mathrm{ED}^{\mathrm{total}}_{\mathrm{exact}}$) is calculated in the exact form [26] to verify the correctness of the long-wave approximation.

Figure 3(a) shows the spectral characteristics of the scattering cross-section of the dielectric torus as well as corresponding multipole contributions. First of all, one can see the coincidence between the SCS and SUM except for the cases where resonances occur at higher orders (e.g., octupoles) that are not accounted for in the SUM. It is obvious that each resonance in the SCS results from the interference (overlapping) of several multipole contributions, where the contribution of the ED is negligible in the entire frequency range of interest. In particular, the dominance of the MD and MQ contributions is observed for the first resonance on the frequency scale, whereas for the second resonance, they are the MD and TD. Notably, the second resonance's frequency is close to the eigenfrequency of the toroidal mode, which manifests itself in the scattered spectra. The toroidal nature of the resonance is also confirmed by the

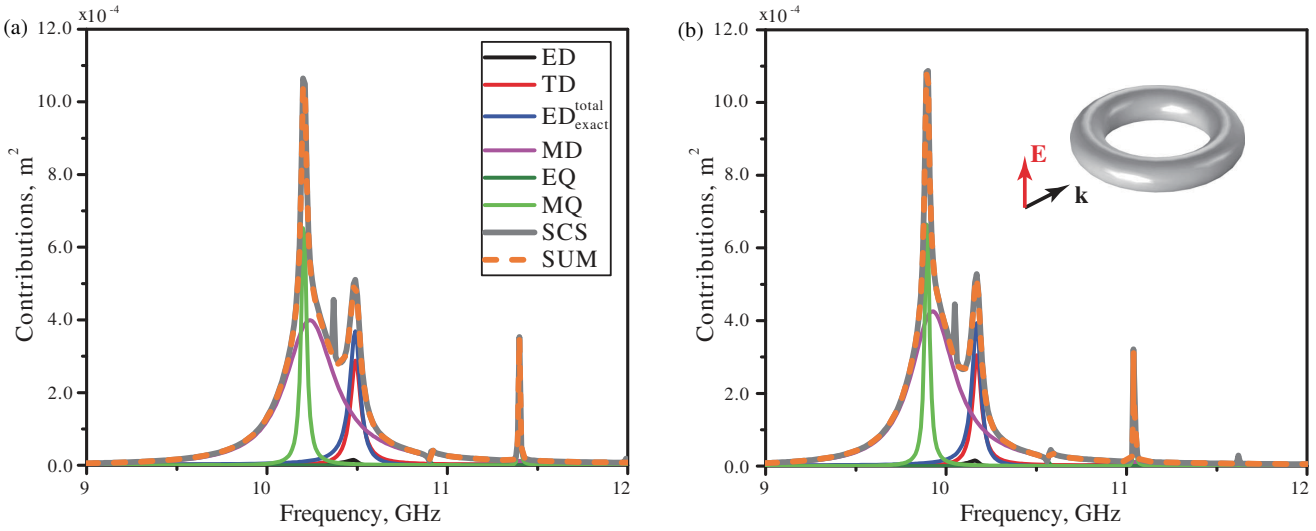

FIGURE 4. Changes in the scattering cross-section (SCS) and corresponding multipole decomposition contributions calculated for a solid torus made of dielectric with the relative permittivity (a) $\varepsilon_{\text{torus}} = 116.85$ and (b) $\varepsilon_{\text{torus}} = 124.57$ corresponding to the rings with $\varepsilon_{\text{eff}} = 60$ composed of $N = 16$ and $N = 12$ disks, respectively. The caption of Fig. 1 lists all other parameters of the structure.

fact that the magnitudes of the TD and $\text{ED}^{\text{total}}_{\text{exact}}$ are almost identical at the resonant frequency. We distinguish this resonant frequency in the figure by a vertical dashed line and denoted as f_{TD}. In general, it can be concluded that the resonance of the toroidal mode in a dielectric torus arises against the background of the MD and MQ contributions, as well as multipoles of the higher order.

Further, the corresponding spectral characteristics of the scattering of the inhomogeneous ring are presented in Figs. 3(b)–(d) for different N and H_d, respectively. Their fundamental difference from the characteristic dependencies for a torus is that the toroidal resonance f_{TD} becomes the lowest-frequency resonance in the spectrum. The contribution of the ED and TD interference approaches the total scattering value SUM, which indicates the separation of the toroidal dipole mode in the ring from other multipole contributions. In other words, when the scattering intensity of three key terms (TD, ED + TD, and SUM) are identical, and the scattering intensity of ED is negligible, the pure TD response is achieved. As secondary effects arise from the properties of the mode, a shift of the resonance to the low-frequency region and an increase in the resonance quality factor appear as N decreases.

Finally, to ensure the completeness of our study, we also calculated the scattering characteristics for a torus made of a material with a relative permittivity corresponding to that of the disks ($\varepsilon_{\text{torus}} = \varepsilon_{\text{disk}}$) obtained above for the structures with $N = 16$ and $N = 12$. The corresponding results are summarized in Fig. 4.

One can see that the characteristic dependencies change little with a moderate increase in permittivity, demonstrating a shift to the low-frequency region where the quality factor tends to increase, as the electromagnetic theory suggests. In general, the observed trends are fully consistent with the parametric studies of a dielectric torus performed earlier in Ref. [53], so we omit the remaining details here.

5. EXPERIMENTAL VALIDATION

The peculiarities of the TD mode excitation in the ring structure are studied by performing its microwave characterization [68, 69]. An experimental sample consists of $N = 6$ resonators fixed on a dielectric substrate. The ring has the radius $R = 4N/\pi$ mm. All disks have the diameter $R_d = 4$ mm and height $H_d = 2.5$ mm. Disks are made from Taizhou Wangling TP commercial ceramics. The relative permittivity of this dielectric material is $\varepsilon_{\text{disk}} = 22 \pm 1$ and the loss factor is $\tan\delta = 1 \times 10^{-3}$. The substrate is made from the ROHACELL®HF rigid foam plate. Its relative permittivity is $\varepsilon_s = 1.1 \pm 0.01$. Our eigenfrequency calculations for the given structure ($\varepsilon_{\text{eff}} \approx 7.56$) predict that the toroidal mode frequency is at $f_{\text{TD}} = 8.31$ GHz.

To obtain the extinction cross-section of the structure based on the optical theorem [70], a two-horn method is carried out. Two antennas (GuanJun GJ-WDRHA-1/18-3/13-S) are placed at each side of the sample as transmitting and receiving antennas, respectively. The distance between the edge of each antenna and the center of the sample is 1.6 m. Then the S_{21} (transmission) coefficient of the electromagnetic waves passing through the ring is recorded by the vector network analyzer (VNA) Rohde & Schwarz ZVA-50. Free space measurement is utilized as a background signal. The forward scattered amplitude is obtained from the difference between the S_{21} coefficient measured for the sample and the background signal. The normalized measured and calculated extinction cross-section is shown in Fig. 5(a). It can be seen that for a given polarization of the incident field, a resonance is observed in the spectral characteristic at the frequency of existence of the toroidal mode of the cluster.

To confirm the manifestation of the toroidal mode in the extinction cross-section of the structure, measurements of the near-field characteristics are carried out. For near-field characterization, a single antenna is set as a transmitting one, whereas

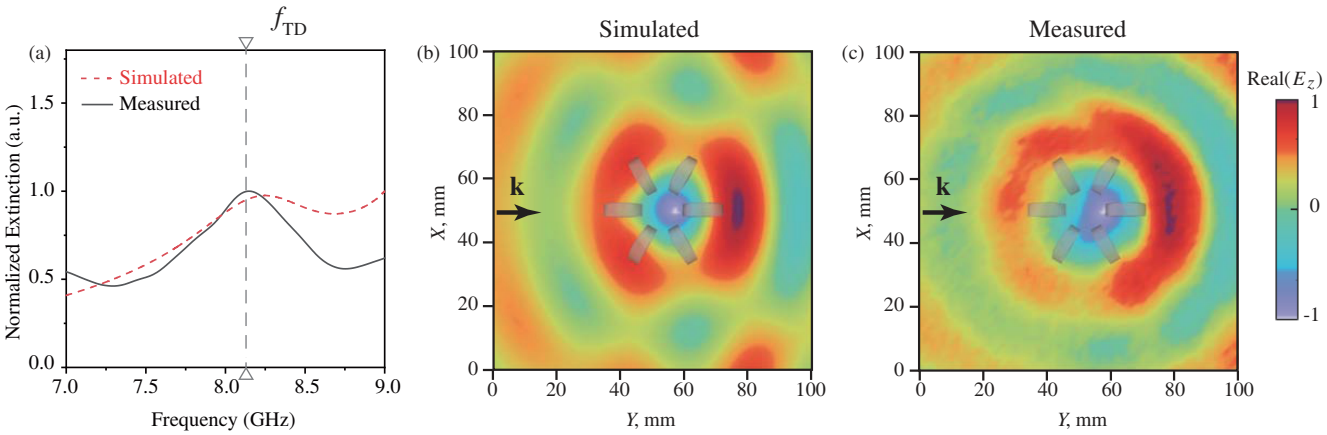

FIGURE 5. (a) Normalized extinction cross-section of the ring structure consisting of six disk-shaped resonators laterally irradiated by a E_z-polarized plane wave, and (b) simulated and (c) measured near-field patterns at $f_{TD} = 8.31$ GHz.

an electric dipole connected to another port of the VNA serves as a receiving probe. The setup aims at acquiring the distribution of a specific component of the electric near-field. The magnitude of the S_{21} coefficient is collected within the frequency band of 7–9 GHz. The scanning area in the pattern is $100 \times 100\,\text{mm}^2$, where the LINBOU near-field imaging system is used to move the probe in the horizontal (x-y) directions with the step of 2 mm.

Figures 5(b) and 5(c) present the simulated and measured distribution patterns of the electric near field (real part of the E_z-component), respectively, at the frequency of appearance of the TD mode in the structure. These color maps are plotted at the distance of 5 mm above the structure scanned in the horizontal plane (where $z = H_d/2 + 5\,\text{mm}$). One can notice that the measured results have a good correspondence with the simulated ones. It confirms the presence of the toroidal mode in the ring structure and the ability of its excitation with the wave of proper polarization.

6. CONCLUSIONS

We have compared the mode composition and scattering characteristics of a homogeneous torus and an inhomogeneous ring from the point of view of the manifestation of a toroidal resonance. Our calculations showed that the toroidal dipole mode in a ring of dielectric disks offers a rich set of properties compared to the homogeneous torus, in particular allowing the toroidal dipole resonance to be separated from other multipole contributions. With fewer disks, the interaction between adjacent disks in the ring is relatively weak, and toroidal modes may not form effectively as the electromagnetic field cannot form the closed loop required for toroidal dipole excitation. The resonances tend to be less sharp, with lower quality factors due to weaker field localization. The moderate number of disks provides optimal coupling. The interaction between disks becomes stronger, and the symmetry is sufficient to support well-defined toroidal modes. In ring structures composed of a large number of disks, properties become similar to the solid torus. In particular, as the number of disks increases, higher-order contributions appear, leading to their overlap which suppresses the quality factor of the toroidal resonance. Regardless of the number of disks, their symmetrical arrangement improves the separation of toroidal modes from other competing resonances. The interplay among geometry, material properties, and excitation conditions plays a crucial role in determining the behavior and utility of this mode.

The inhomogeneous distribution of material properties in the ring enhances the field localization within certain regions of the structure. This localization reduces radiative losses by confining more energy within the resonators. The inhomogeneity also creates a spectral separation between the toroidal mode and competing modes, reducing interference and enhancing the purity of the toroidal resonance. In contrast, in a homogeneous torus, the field distribution is uniform and less localized, leading to increased radiative losses. Competing modes (e.g., dipolar or quadrupolar modes) can overlap or interfere with the toroidal mode, increasing dissipation and lowering the quality factor.

Toroidal modes can enhance sensitivity for microwave-based biosensors, enabling the detection of biological and chemical substances with high precision. Their strong field localization can be used in devices that rely on nonlinear materials for switching and modulation. Their spectral selectivity may improve the resolution and sensitivity of microwave imaging systems, which are used in medical diagnostics, security screening, and non-destructive testing.

The studied properties and manifestation of the toroidal dipole mode in the microwave range can be scaled to higher frequencies when a sufficiently large permittivity for the constitutive particles is provided. However, if the permittivity is not large enough, the contribution of the LWA electric dipole moment will increase, leading to a decrease in the quality factor of the toroidal resonance.

ACKNOWLEDGEMENT

T.W. is grateful for the support from Jilin University, China. A.B.E. acknowledges the Deutsche Forschungsgemeinschaft (DFG, German Research Foundation) under Germany's Excel-

lence Strategy within the Cluster of Excellence PhoenixD (EXC 2122, Project ID 390833453).

APPENDIX A. BASIC MULTIPOLE EXPANSION

In our paper, we use the approach to describe the multipole response of material systems proposed recently in [26, 65]. In this framework, it is considered that multipole moments in radiation and scattering problems can be introduced by two methods: either by expanding the delta function in a Taylor series in the integral determining the induced currents in the system or by expanding the radiated (scattered) fields in the far-field zone in terms of vector spherical harmonics (which is called 'exact' [65]). If spherical (exact) multipoles are expanded by the parameter of the ratio of the system size to the radiation wavelength, then the multipoles from the delta-function expansion are obtained in terms of this expansion. This representation of multipole moments is called 'long-wave approximation' (LWA) [26].

Taking into account several first spherical multipoles in the Cartesian basis (the exact multipoles), the scattering cross-section can be presented as [26, 66]

$$\sigma_{\text{sca}} \simeq \frac{k_0^4}{6\pi\varepsilon_0^2|\mathbf{E}|^2}|\mathbf{p}|^2 + \frac{k_0^6\varepsilon_s}{720\pi\varepsilon_0^2|\mathbf{E}|^2}\sum_{\alpha\beta}|Q_{\alpha\beta}|^2 + \frac{k_0^4\varepsilon_s\mu_0}{6\pi\varepsilon_0|\mathbf{E}|^2}|\mathbf{m}|^2 + \frac{k_0^6\varepsilon_s^2\mu_0}{80\pi\varepsilon_0|\mathbf{E}|^2}\sum_{\alpha\beta}|M_{\alpha\beta}|^2, \quad \text{(A1)}$$

where k_0 is the wavenumber in vacuum; ε_0 is the vacuum dielectric constant; ε_s is the relative dielectric constant of the surrounding medium; μ_0 is the vacuum permeability; $\mathbf{E}$ is the electric field amplitude of the incident plane wave; $\mathbf{p}$ and $\mathbf{m}$ are the vectors of the exact electric and magnetic dipole moments, respectively; and $\hat{Q}$ and $\hat{M}$ are the 3×3 tensors of the exact electric and magnetic quadrupole moments (the integral expressions determining the exact multipole moments are not presented here and can be found in Table 2 in [26], and the only difference is that for Eq. (A1) the magnetic quadrupole moment must be taken with a coefficient reduced by three times).

For the scatterer smaller than the incident wavelength λ (in our problem, it can be related to the major radius of the torus, $2Rk_0\sqrt{\varepsilon_{\text{torus}}} \lesssim 1$), the expressions for the exact multipoles can be represented in the long-wavelength multipole approximation (LWA) [70].

$$\begin{aligned}\sigma_{\text{sca}} &\simeq \frac{k_0^4}{6\pi\varepsilon_0^2|\mathbf{E}|^2}\left|\mathbf{p}_0+\eta\mathbf{T}\right|^2 + \frac{k_0^6\varepsilon_s}{720\pi\varepsilon_0^2|\mathbf{E}|^2}\sum_{\alpha\beta}\left|Q^0_{\alpha\beta}\right|^2 \\ &+ \frac{k_0^4\varepsilon_s\mu_0}{6\pi\varepsilon_0|\mathbf{E}|^2}\left|\mathbf{m}_0\right|^2 + \frac{k_0^6\varepsilon_s^2\mu_0}{80\pi\varepsilon_0|\mathbf{E}|^2}\sum_{\alpha\beta}\left|M^0_{\alpha\beta}\right|^2 \\ &\equiv (\text{ED}+\text{TD})+\text{EQ}+\text{MD}+\text{MQ}, \quad \text{(A2)}\end{aligned}$$

where $\eta = ik_0\varepsilon_s c^{-1}$. In the LWA, we omit the higher-order terms (the mean-square radii) for all contributions, while the electric $\mathbf{p}_0$ and toroidal $\mathbf{T}$ dipole moments, respectively, are expressed as:

$$\mathbf{p}_0 = \frac{i}{\omega}\int_V \mathbf{J_D}\, d\mathbf{r}, \quad \text{(A3)}$$

$$\mathbf{T} = \frac{1}{10}\int_V [(\mathbf{r}\cdot\mathbf{J_D})\mathbf{r} - 2r^2\mathbf{J_D}]d\mathbf{r}, \quad \text{(A4)}$$

where V is the total volume of the particles in the system; ω is the angular frequency of the incident wave; and the time dependence $\exp(-i\omega t)$ is assumed.

For the ring system composed of N disks $V = \sum_{n=1}^{N} V_n$, where n is the index running over the disks. Explicit definitions of the rest of the multipoles entering the LWA can be found in Table 1 of Ref. [60].

In our simulation procedure implemented in COMSOL we first calculate the induced displacement current density $\mathbf{J_D}(\mathbf{r}) = -i\omega\varepsilon_0(\varepsilon-\varepsilon_s)\mathbf{E}(\mathbf{r})$ in the disks and then the total scattering cross-section without application of the multipole decomposition method, and second, using obtained $\mathbf{J_D}(\mathbf{r})$, the multipole moments and their contributions to the scattering cross-section are determined in the LWA conditions. Here $\mathbf{E}(\mathbf{r})$ is the total electric field in the considered system. All multipole moments considered above are located at the coordinate-system origin coincident with the mass center of the structure.

APPENDIX B. SECONDARY MULTIPOLE DECOMPOSITION

The main purpose of involving the secondary multipole decomposition (SMD) method is to obtain a representation of the multipole moments of the ring system via the multipole moments of its constitutive disks. Here we follow the procedure introduced in Refs. [59, 60].

Using the replacement $\mathbf{r} = \mathbf{r}_n + \mathbf{r}'_n$ of the radius-vector $\mathbf{r}$ defined concerning the center of mass of the cluster, where $\mathbf{r}_n$ $(n = 1\ldots N)$ is the radius-vectors of disk's centers, and $\mathbf{r}'_n$ is the radius-vector of any point inside corresponding disk to its center (see Fig. 9 in [59]), the vector of the TD moment of a whole ring system can be written as:

$$\mathbf{T} = \sum_{n=1}^{N}\left\{\mathbf{T}_0(\mathbf{r}_n) + \mathbf{T}_n + \frac{4}{5}[\mathbf{r}_n\times\mathbf{m}_n] + \mathbf{I}(\mathbf{r}_n)\right\}, \quad \text{(B1)}$$

where

$$\mathbf{T}_0(\mathbf{r}_n) = \frac{\omega}{10i}\left[(\mathbf{r}_n\cdot\mathbf{p}_n)\mathbf{r}_n - 2r_n^2\mathbf{p}_n\right] \quad \text{(B2)}$$

is the TD moment at the cluster mass center associated with the LWA electric dipole moment

$$\mathbf{p}_n = \frac{i}{\omega}\int_{V_n}\mathbf{J_D}d\mathbf{r}_n$$

of the subsystem (disk) with the number n,

$$\mathbf{T}_n = \frac{1}{10}\int_{V_n}\left[(\mathbf{r}'_n\cdot\mathbf{J_D})\mathbf{r}'_n - 2(r'_n)^2\mathbf{J_D}\right]d\mathbf{r}'_n$$

and

$$\mathbf{m}_n = \frac{1}{2}\int_{V_n} [\mathbf{r}'_n \times \mathbf{J_D}] d\mathbf{r}'_n$$

are the TD moment and the LWA MD moment of the same disk with the number n calculated concerning its mass center, respectively, and

$$\mathbf{I}(\mathbf{r}_n) = \frac{1}{10}\int_{V_n} [(\mathbf{r}'_n \cdot \mathbf{J_D})\mathbf{r}_n - 3(\mathbf{r}_n \cdot \mathbf{J_D})\mathbf{r}'_n]\, d\mathbf{r}'_n \qquad \text{(B3)}$$

is an additional integral term that accounts for the offset of the n-th particle from the cluster's mass center.

REFERENCES

[1] Zhao, Q., J. Zhou, F. Zhang, and D. Lippens, "Mie resonance-based dielectric metamaterials," *Materials Today*, Vol. 12, No. 12, 60–69, 2009.

[2] Won, R., "Into the 'Mie-tronic' era," *Nature Photonics*, Vol. 13, No. 9, 585–587, 2019.

[3] Kivshar, Y., "The rise of Mie-tronics," *Nano Letters*, Vol. 22, No. 9, 3513–3515, 2022.

[4] Kruk, S. and Y. Kivshar, "Functional meta-optics and nanophotonics governed by Mie resonances," *ACS Photonics*, Vol. 4, No. 11, 2638–2649, 2017.

[5] Xiao, S., T. Wang, T. Liu, C. Zhou, X. Jiang, and J. Zhang, "Active metamaterials and metadevices: A review," *Journal of Physics D: Applied Physics*, Vol. 53, No. 50, 503002, Sep. 2020.

[6] Babicheva, V. E. and A. B. Evlyukhin, "Mie-resonant metaphotonics," *Advances in Optics and Photonics*, Vol. 16, No. 3, 539–658, Sep. 2024.

[7] Evlyukhin, A. B., S. M. Novikov, U. Zywietz, R. L. Eriksen, C. Reinhardt, S. I. Bozhevolnyi, and B. N. Chichkov, "Demonstration of magnetic dipole resonances of dielectric nanospheres in the visible region," *Nano Letters*, Vol. 12, No. 7, 3749–3755, 2012.

[8] Kuznetsov, A. I., A. E. Miroshnichenko, Y. H. Fu, J. Zhang, and B. Luk'Yanchuk, "Magnetic light," *Scientific Reports*, Vol. 2, No. 1, 492, 2012.

[9] Zhang, F., L. Kang, Q. Zhao, J. Zhou, and D. Lippens, "Magnetic and electric coupling effects of dielectric metamaterial," *New Journal of Physics*, Vol. 14, No. 3, 033031, Mar. 2012.

[10] Evlyukhin, A. B., C. Reinhardt, and B. N. Chichkov, "Multipole light scattering by nonspherical nanoparticles in the discrete dipole approximation," *Physical Review B*, Vol. 84, No. 23, 235429, Dec. 2011.

[11] Jackson, J. D., *Classical Electrodynamics*, John Wiley & Sons, 2021.

[12] Hergert, W. and T. Wriedt, *The Mie Theory: Basics and Applications*, Springer, 2012.

[13] Kajfez, D. and P. Guillon, *Dielectric Resonators*, 2nd ed., Noble Publishing Corporation, 1998.

[14] Luk, K. M. and K. W. Leung, *Dielectric Resonator Antennas*, Research Studies Press, 2003.

[15] Mongia, R. K. and P. Bhartia, "Dielectric resonator antennas — A review and general design relations for resonant frequency and bandwidth," *International Journal of Microwave and Millimeter-Wave Computer-Aided Engineering*, Vol. 4, No. 3, 230–247, 1994.

[16] Trubin, A., *Lattices of Dielectric Resonators*, Springer, 2015.

[17] Marinov, K., A. D. Boardman, V. A. Fedotov, and N. Zheludev, "Toroidal metamaterial," *New Journal of Physics*, Vol. 9, No. 9, 324, Sep. 2007.

[18] Basharin, A. A., M. Kafesaki, E. N. Economou, C. M. Soukoulis, V. A. Fedotov, V. Savinov, and N. I. Zheludev, "Dielectric metamaterials with toroidal dipolar response," *Physical Review X*, Vol. 5, No. 1, 011036, Mar. 2015.

[19] Tasolamprou, A. C., O. Tsilipakos, M. Kafesaki, C. M. Soukoulis, and E. N. Economou, "Toroidal eigenmodes in all-dielectric metamolecules," *Physical Review B*, Vol. 94, No. 20, 205433, Nov. 2016.

[20] Tuz, V. R., V. V. Khardikov, and Y. S. Kivshar, "All-dielectric resonant metasurfaces with a strong toroidal response," *ACS Photonics*, Vol. 5, No. 5, 1871–1876, 2018.

[21] Xu, S., A. Sayanskiy, A. S. Kupriianov, V. R. Tuz, P. Kapitanova, H.-B. Sun, W. Han, and Y. S. Kivshar, "Experimental observation of toroidal dipole modes in all-dielectric metasurfaces," *Advanced Optical Materials*, Vol. 7, No. 4, 1801166, 2019.

[22] Dmitriev, V., A. S. Kupriianov, S. D. S. Santos, and V. R. Tuz, "Symmetry analysis of trimer-based all-dielectric metasurfaces with toroidal dipole modes," *Journal of Physics D: Applied Physics*, Vol. 54, No. 11, 115107, Jan. 2021.

[23] Dmitriev, V., S. D. S. Santos, A. B. Evlyukhin, A. S. Kupriianov, and V. R. Tuz, "Toroidic and antitoroidic orders in hexagonal arrays of dielectric trimers: Magnetic group approach," *Physical Review B*, Vol. 103, No. 16, 165402, Apr. 2021.

[24] Basharin, A. A., E. Zanganeh, A. K. Ospanova, P. Kapitanova, and A. B. Evlyukhin, "Selective superinvisibility effect via compound anapole," *Physical Review B*, Vol. 107, No. 15, 155104, 2023.

[25] Fernandez-Corbaton, I., S. Nanz, and C. Rockstuhl, "On the dynamic toroidal multipoles from localized electric current distributions," *Scientific Reports*, Vol. 7, No. 1, 7527, 2017.

[26] Alaee, R., C. Rockstuhl, and I. Fernandez-Corbaton, "An electromagnetic multipole expansion beyond the long-wavelength approximation," *Optics Communications*, Vol. 407, 17–21, 2018.

[27] Huang, Y.-W., W. T. Chen, P. C. Wu, V. A. Fedotov, N. I. Zheludev, and D. P. Tsai, "Toroidal lasing spaser," *Scientific Reports*, Vol. 3, No. 1, 1237, 2013.

[28] Miroshnichenko, A. E., A. B. Evlyukhin, Y. F. Yu, R. M. Bakker, A. Chipouline, A. I. Kuznetsov, B. Luk'yanchuk, B. N. Chichkov, and Y. S. Kivshar, "Nonradiating anapole modes in dielectric nanoparticles," *Nature Communications*, Vol. 6, No. 1, 8069, 2015.

[29] Ahmadivand, A., B. Gerislioglu, and Z. Ramezani, "Generation of magnetoelectric photocurrents using toroidal resonances: A new class of infrared plasmonic photodetectors," *Nanoscale*, Vol. 11, No. 27, 13 108–13 116, 2019.

[30] Marinov, K. and V. A. Fedotov, "Gyrotropy and permittivity sensing driven by toroidal response," *New Journal of Physics*, Vol. 25, No. 2, 023030, Feb. 2023.

[31] Smirnova, D. and Y. S. Kivshar, "Multipolar nonlinear nanophotonics," *Optica*, Vol. 3, No. 11, 1241–1255, Nov. 2016.

[32] Ahmadivand, A., B. Gerislioglu, R. Ahuja, and Y. K. Mishra, "Toroidal metaphotonics and metadevices," *Laser & Photonics Reviews*, Vol. 14, No. 11, 1900326, 2020.

[33] Canós Valero, A., D. Borovkov, A. Kalganov, A. Dudnikova, M. Sidorenko, P. Dergachev, E. Gurvitz, L. Gao, V. Bobrovs, A. Miroshnichenko, and A. S. Shalin, "On the existence of pure, broadband toroidal sources in electrodynamics," *Laser & Photonics Reviews*, Vol. 18, No. 4, 2200740, 2024.

[34] Laurin, P., "Scattering by a torus," Ph.D. dissertation, University of Michigan, Ann Arbor, MI, USA, 1967.

[35] Brambilla, M. and U. Finzi, "Electro-magnetic eigenmodes of the toroidal cavity," *IEEE Transactions on Plasma Science*, Vol. 2, No. 3, 112–114, 1974.

[36] Janaki, M. S. and B. Dasgupta, "Eigenmodes for electromagnetic waves propagating in a toroidal cavity," *IEEE Transactions on Plasma Science*, Vol. 18, No. 1, 78–85, 1990.

[37] Kark, K. W., "Perturbation analysis of electromagnetic eigenmodes in toroidal waveguides," *IEEE Transactions on Microwave Theory and Techniques*, Vol. 39, No. 4, 631–637, 1991.

[38] Schupfer, N., "Axisymmetric electromagnetic eigenmodes of plasma-filled toroidal resonators," *IEEE Transactions on Plasma Science*, Vol. 19, No. 5, 906–911, 1991.

[39] Menachem, Z., N. I. Croitoru, and J. Aboudi, "Improved mode model for infrared wave propagation in a toroidal dielectric waveguide and applications," *Optical Engineering*, Vol. 41, No. 9, 2169–2180, 2002.

[40] Scharstein, R. W. and H. B. Wilson, "Electrostatic excitation of a conducting toroid: Exact solution and thin-wire approximation," *Electromagnetics*, Vol. 25, No. 1, 1–19, 2005.

[41] Talebi, N., M. Shahabadi, and C. V. Hafner, "Analysis of a lossy microring using the generalized multipole technique," *Progress In Electromagnetics Research*, Vol. 66, 287–299, 2006.

[42] Bibby, M. M., C. M. Coldwell, and A. F. Peterson, "A high order numerical investigation of electromagnetic scattering from a torus and a circular loop," *IEEE Transactions on Antennas and Propagation*, Vol. 61, No. 7, 3656–3661, 2013.

[43] Zakeri-Khatir, H. and F. M. Aghamir, "Cutoff frequency of toroidal plasma waveguide," *Physics of Plasmas*, Vol. 22, No. 2, 022121, 2015.

[44] Muscia, R., "Evaluation of forces and torques generated by toroidal helicoidal magnetic fields," *Progress In Electromagnetics Research B*, Vol. 74, 37–59, 2017.

[45] Sukharevsky, O., V. Vasilets, and V. Misailov, "Calculation method of electromagnetic waves scattering by dielectric toroid meteorological formations," *Radioelectronics and Communications Systems*, Vol. 63, No. 11, 596–605, 2020.

[46] Xu, J. and J. L. Han, "The huge magnetic toroids in the Milky Way halo," *The Astrophysical Journal*, Vol. 966, No. 2, 240, May 2024.

[47] Cap, F. and R. Deutsch, "Toroidal resonators for electromagnetic waves," *IEEE Transactions on Microwave Theory and Techniques*, Vol. 26, No. 7, 478–486, 1978.

[48] Arfken, G., *Mathematical Methods for Physicists*, 2nd ed., Academic Press, Orlando, FL, 1970.

[49] Dutta, C. M., T. A. Ali, D. W. Brandl, T.-H. Park, and P. Nordlander, "Plasmonic properties of a metallic torus," *The Journal of Chemical Physics*, Vol. 129, No. 8, 084706, 2008.

[50] Shi, Q., Z. Yu, Y. Liu, H. Gong, H. Yin, W. Zhang, J. Liu, and Y. Peng, "Plasmonics properties of nano-torus: An FEM method," *Optics Communications*, Vol. 285, No. 21-22, 4542–4548, 2012.

[51] Garapati, K. V., M. Salhi, S. Kouchekian, G. Siopsis, and A. Passian, "Poloidal and toroidal plasmons and fields of multilayer nanorings," *Physical Review B*, Vol. 95, No. 16, 165422, Apr. 2017.

[52] Pedersen, T. G., "Plasmons and magnetoplasmon resonances in nanorings," *Physical Review B*, Vol. 103, No. 8, 085419, Feb. 2021.

[53] Liu, L. and L. Ge, "Toroidal dipole resonances by a subwavelength all-dielectric torus," *Optics Express*, Vol. 30, No. 5, 7491–7500, Feb. 2022.

[54] Liang, Y., D. P. Tsai, and Y. Kivshar, "From local to nonlocal high-Q plasmonic metasurfaces," *Physical Review Letters*, Vol. 133, No. 5, 053801, Jul. 2024.

[55] Kaelberer, T., V. A. Fedotov, N. Papasimakis, D. P. Tsai, and N. I. Zheludev, "Toroidal dipolar response in a metamaterial," *Science*, Vol. 330, No. 6010, 1510–1512, 2010.

[56] Papasimakis, N., V. A. Fedotov, V. Savinov, T. A. Raybould, and N. I. Zheludev, "Electromagnetic toroidal excitations in matter and free space," *Nature Materials*, Vol. 15, No. 3, 263–271, 2016.

[57] Wu, T., A. B. Evlyukhin, and V. R. Tuz, "Bonding and antibonding electromagnetic coupling in two interacting toroidal metamolecules," *Physical Review B*, Vol. 110, No. 11, 115408, Sep. 2024.

[58] Wu, T., A. B. Evlyukhin, and V. R. Tuz, "Toroidal mode trapping in a magnetic meta-molecule," *Journal of Physics D: Applied Physics*, Vol. 57, No. 50, 505301, Sep. 2024.

[59] Tuz, V. R., V. Dmitriev, and A. B. Evlyukhin, "Antitoroidic and toroidic orders in all-dielectric metasurfaces for optical near-field manipulation," *ACS Applied Nano Materials*, Vol. 3, No. 11, 11 315–11 325, 2020.

[60] Tuz, V. R. and A. B. Evlyukhin, "Polarization-independent anapole response of a trimer-based dielectric metasurface," *Nanophotonics*, Vol. 10, No. 17, 4373–4383, 2021.

[61] Maxwell-Garnett, J. C., "XII. Colours in metal glasses and in metallic films," *Philosophical Transactions of the Royal Society of London. Series A, Containing Papers of a Mathematical or Physical Character*, Vol. 203, No. 359-371, 385–420, 1904.

[62] Giannakopoulou, T., D. Niarchos, and C. Trapalis, "Experimental investigation of electric and magnetic responses in composites with dielectric resonator inclusions at microwave frequencies," *Applied Physics Letters*, Vol. 94, No. 24, 242506, 2009.

[63] Bronshtein, I. N., K. A. Semendyayev, G. Musiol, *et al.*, *Handbook of Mathematics*, 5th ed., Springer-Verlag, Berlin, 2007.

[64] Yushanov, S., J. S. Crompton, and K. C. Koppenhoefer, "Mie scattering of electromagnetic waves," in *Proceedings of the COMSOL Conference*, Vol. 116, 1–7, Boston, MA, USA, 2013.

[65] Alaee, R., C. Rockstuhl, and I. Fernandez-Corbaton, "Exact multipolar decompositions with applications in nanophotonics," *Advanced Optical Materials*, Vol. 7, No. 1, 1800783, 2019.

[66] Evlyukhin, A. B. and B. N. Chichkov, "Multipole decompositions for directional light scattering," *Physical Review B*, Vol. 100, No. 12, 125415, Sep. 2019.

[67] Poleva, M., K. Frizyuk, K. Baryshnikova, A. Evlyukhin, M. Petrov, and A. Bogdanov, "Multipolar theory of bianisotropic response of meta-atoms," *Physical Review B*, Vol. 107, No. 4, L041304, 2023.

[68] Kupriianov, A. S. and V. R. Tuz, "Microwave approach to study resonant features of all-dielectric metasurfaces," in *2019 Photonics & Electromagnetics Research Symposium — Fall (PIERS — Fall)*, 866–870, Xiamen, China, Dec. 2019.

[69] Wu, T., A. B. Evlyukhin, and V. R. Tuz, "Microwave characterization of exotic resonant states in dielectric resonators," in *2024 IEEE 4th International Conference on Electronic Technology, Communication and Information (ICETCI)*, 461–465, Changchun, China, May 2024.

[70] Evlyukhin, A. B., T. Fischer, C. Reinhardt, and B. N. Chichkov, "Optical theorem and multipole scattering of light by arbitrarily shaped nanoparticles," *Physical Review B*, Vol. 94, No. 20, 205434, 2016.